 MCB, vol.1, no.3, pp.169-180, 2004

Nonlinear Elastic and Viscoelastic Deformation of the Human Red Blood Cell with Optical Tweezers

J. P. Mills[1], L. Qie[2], M. Dao[1], C. T. Lim[2] and S. Suresh[1, 3]

Abstract: Studies of the deformation characteristics of single biological cells can offer insights into the connections among mechanical state, biochemical response and the onset and progression of diseases. Deformation imposed by optical tweezers provides a useful means for the study of single cell mechanics under a variety of well-controlled stress-states. In this paper, we first critically review recent advances in the study of single cell mechanics employing the optical tweezers method, and assess its significance and limitations in comparison to other experimental tools. We then present new experimental and computational results on shape evolution, force–extension curves, elastic properties and viscoelastic response of human red blood cells subjected to large elastic deformation using optical tweezers. Potential applications of the methods examined here to study diseased cells are also briefly addressed.

1 Introduction and overview

Optical tweezers are finding increasing application in the study of single biological cells. Ashkin et al (1987) used infrared laser beams to optically trap and manipulate single cells. An optical trap was used by Svoboda et al (1992) to isolate the membrane skeleton from a red blood cell, which was treated with a non-ionic detergent, so as to study the effect of ionic strength on the contraction of the spectrin network. Bronkhorst et al (1995) employed triple traps to deform and to explore shape recovery of red blood cells.

Direct tensile stretching of the human red blood cell using optical tweezers to extract elastic properties was first reported by Hénon et al (1999) who attached two silica beads non-specifically to diametrically opposite ends of the cell, trapped both beads with laser beams, and imposed tensile elastic deformation on the cell by moving the trapped beads in opposite directions. Forces were calibrated by subjecting a trapped bead to counter flow following the procedures outlined by Svoboda and Block (1994) and Simmons et al (1996). Stokes' law was used to estimate the force on the trapped bead from known fluid velocity. With a 1.064 μm Nd:YAG laser beam of 605 mW maximum emission power and silica beads 2.1 μm in diameter, they imposed maximum tensile forces that were estimated to be 56 pN on discocytic and osmotically swollen, nearly spherical cells. By employing simple analytical expressions based on two-dimensional linear elastic, small deformation, idealization of the cell, they examined variations in only the transverse diameter of the cell with applied force, and ignored possible contributions to deformation arising from the bending stiffness of the cell membrane and cytoskeleton. Finite contact between the beads and the cell membrane during stretching by optical tweezers was also not considered. The in-plane shear modulus of the cell membrane was estimated from this approach to be 2.5 ± 0.4 μN/m. This estimate is lower than the range of shear modulus values of 4 to 10 μN/m obtained from a number of independent investigations which employed the more commonly known micropipette aspiration technique (Evans and Skalak, 1980; Hochmuth and Waugh, 1987; Discher et al, 1998; Boal, 2002). Studies by the same group (Lenormand et al, 2001) employing triple bead optical tweezers measurements showed that the area expansion modulus and shear modulus of red blood cells were higher in an isotonic buffer than in a low hypotonic buffer.

Sleep et al (1999) also estimated elastic properties of the human red blood cells by optical tweezers where two polystyrene latex beads of 1 μm diameter were trapped using a 1.047 μm Nd:YLF laser beam. In this experiment, one bead was held fixed and the other moved with a second trap to induce tensile deformation in the cell.

[1] Department of Materials Science and Engineering.
[2] Division of Bioengineering, National University of Singapore, Singapore 117576, Singapore.
[3] Division of Biological Engineering (e-mail: ssuresh@mit.edu), Massachusetts Institute of Technology, Cambridge, MA 02139, USA.

Trap stiffness was estimated from the Brownian motion of the trapped bead. The variation of imposed force, up to a maximum of 20 pN, as a function of the transverse diameter, was reported for permeabilized spherical ghost cells whose deformation at a given force was about one half that of discocytic and osmotically swollen spherical cells. By invoking an axisymmetric cell model of Parker and Winlove (1999), they estimated the in-plane shear modulus from optical tweezers studies to be nearly two orders of magnitude larger than those reported by Hénon et al (1999).

All of the foregoing studies of cell deformation by optical tweezers involve primarily small elastic deformation at low applied forces. The analyses of deformation for extracting elastic properties also invoke rather severe assumptions on cell shape (e.g., idealization of a biconcave cell as a two-dimensional planar disc by Hénon et al (1999), and neglect of the effects of the relatively large contact region between the cell and the beads in this study and in the one by Sleep et al (1999)). Studies of deformation conditions at larger strain levels inevitably require much higher forces, which are conceptually feasible to obtain using the optical tweezers method. In fact, a study of unfolding of titin molecules by Kellermayer et al (1998) reported an estimated stretching force in excess of 400 pN using optical tweezers where a 1046 nm Nd:YAG laser with a maximum power of 1.5 W was used to trap a 3 μm diameter latex bead and where the force calibration was performed using the Stokes' law method.

In principle, the optical tweezers method affords several potential advantages for the study of deformation of single biological cells. (1) It provides a means to impose simple and well-controlled stress states, such as direct tensile stretching in small or large deformation, to biological cells. In this sense, it is complementary to, and conceptually simpler to interpret than, the widely used micropipette aspiration method (Evans and Skalak 1980, Fung 1993). (2) The stress state imposed on the cell can be systematically varied by employing multiple beads which are attached to cell membranes, whereby the constitutive response of the cell membrane and cytoskeleton can be probed for different chemical and biological conditions. (3) Optical tweezers stretching of cells in one or more directions is also amenable to three-dimensional computational simulations which can be used to guide and interpret experimental observations. (4) The relaxation response of the stretched cell upon release of the tensile stretch in the optical tweezers experiments can also be used to extract the viscoelastic response of the cell. (5) This method further provides a possible means to investigate systematically the effects of the progression of a disease state, such as infestation of the red blood cell with *Plasmodium falciparum* malaria parasite, on the deformation characteristics and elastic and viscoelastic properties of the cell membrane (Mills et al, 2004). Possible complications arising from micropipette aspiration of such infected cells, such as stress concentration at the ends of the micropipette and adhesion of the infected cell to the inner walls of the micropipette, can potentially be circumvented in the optical tweezers method. Despite these advantages, uncertainties exist in the calibration of the force imposed on the cell by the optical tweezers method, which is in the picoNewton to several hundred picoNewton range. Such complications have led to considerable variation and scatter in the experimental data reported previously in the literature. A comparison of the optical tweezers method with other techniques available for the study of mechanics of single cells and populations of cells can be found in recent reviews (Bao and Suresh, 2003; Van Vliet et al, 2003).

The possibility of inducing large elastic deformation in human red blood cells using optical tweezers was also demonstrated recently (see the papers by Dao et al., 2003; Lim et al, 2004 along with the attendant corrigenda). Here, forces as high as about 193 ± 20 pN were estimated to result in strains on the order of 100% in the cell.

In the present paper, we review these developments from earlier work and present refinements and updates to the experimental method and force calibration. Furthermore, a fully nonlinear constitutive model based on a three-stage neo-Hookean elastic response is presented along with new computational simulations of cell deformation to systematically probe the large deformation response of the red blood cell. The predictions are compared with new experimental data obtained in this work. In addition, the values of elastic properties and characteristic time for viscoelastic relaxation extracted from the present optical tweezers experiments on normal human red blood cells are shown to be within the range of values obtained from prior experimental studies that employed the micropipette aspiration technique.

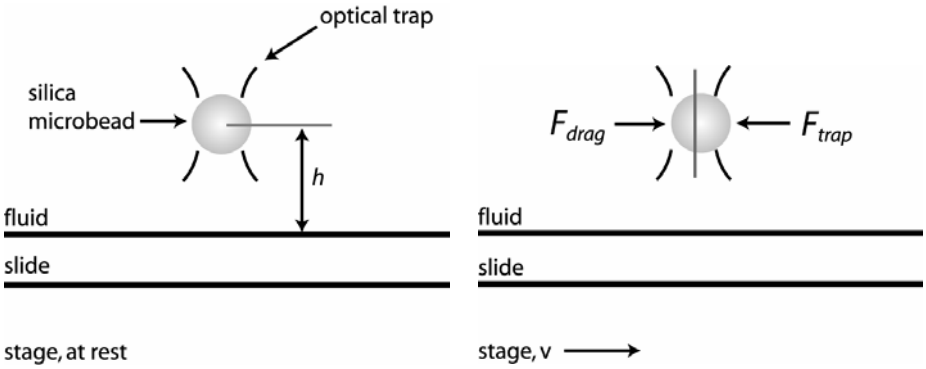

Figure 1 : Calibration of the optical trap using an escape force method (Svoboda and Block, 1994). A silica microbead, 4.12 μm in diameter, is trapped in fluid (PBS and bovine serum albumin, BSA) at a measured height, h = 3 μm, above the slide surface. As the microscope stage and fixed slide are translated, the fluid exerts a viscous drag force on the trapped bead. When the viscous drag force is just equal to the escape force, the bead will escape the trap.

2 Experimental Method

The optical tweezers system used here comprises a single-bead gradient optical trap. It incorporates an inverted microscope (Leica Microsystems, Wetzlar, Germany) and a laser module (LaserTweezers, Cell Robotics, Inc.). The trapping beam is a 1064 nm Nd:YAG laser with a maximum power of 1.5 W. Focusing the laser through an oil immersion lens (100× magnification) forms the optical trap. Silica beads, 4.12 μm in diameter (Bangs Laboratories, USA), are optically trapped by the laser to perform stretch tests. The relatively high laser power and large bead diameter facilitate the exertion of forces on the cell that are about three to six times greater than those reported by the earlier studies (Hénon et al. 1999, Sleep et al. 1999).

2.1 Force calibration

The optical tweezers system is calibrated using an escape force method (Svoboda and Block, 1994). In this technique, the force required to dislodge a trapped microbead is calibrated against a known viscous drag force. The calibration procedure involves trapping a silica microbead in fluid (phosphate-buffered saline (PBS) and bovine serum albumin (BSA)) at a measured height, h = 3 μm, above the glass slide surface. The fluid and height of the trapped bead from the slide surface are kept unchanged throughout calibration and mechanical deformation. As the microscope stage is translated, the fluid exerts a viscous drag force on the trapped bead, as shown in Fig. 1. The viscous drag force equals the trapping force when the bead just escapes the trap. From the stage velocity, ν, at the point of escape of the trapped bead, the drag force, which is the opposite of the escape force, is estimated as

$$F = \beta v. \tag{1}$$

The viscous drag coefficient, β, for a spherical bead located near a wall is described by Faxen's Law (Svoboda and Block, 1994),

$$\beta = \frac{6\pi\eta r}{1 - \frac{9}{16}(r/h) + \frac{1}{8}(r/h)^3 - \frac{4}{256}(r/h)^4 - \frac{1}{16}(r/h)^5}, \tag{2}$$

where, for the present experiments, the bead radius, r = 2.06 μm, height of the bead above the wall, h = 3 μm, and fluid viscosity, η = 0.0013 Pa·s. Notice that Eq. (1) takes the form of Stokes' law, $F = 6\pi r\eta\nu$, for a bead located far from the wall.

The stage-movement technique described here differs somewhat from the fluid-chamber technique used in our earlier work (Dao et al., 2003; Lim et al., 2004). The fluid-chamber technique imposes a viscous drag force by flowing fluid through a narrow channel where a microbead is trapped. Fluid velocity, estimated by tracking the speed of untrapped beads, is used with Eq. (1) to determine the escape force. However, this method is limited by our optical tweezers set-up. First, untrapped beads used to determine fluid velocity should be flowing at the same height above the slide as the trapped bead.

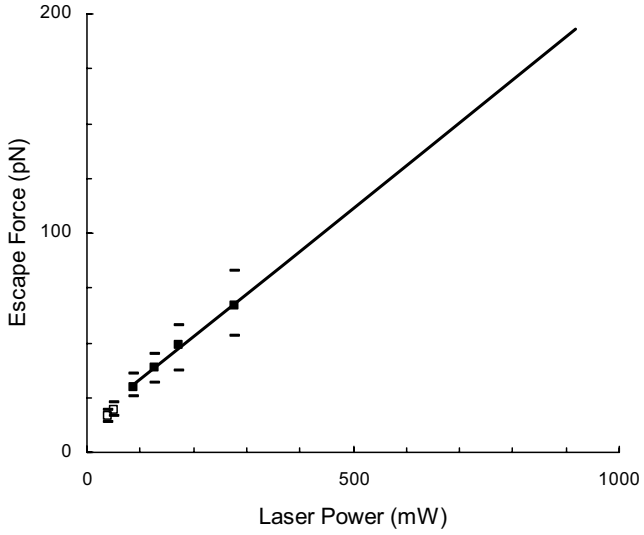

Figure 2 : Force calibration plot showing the variation of trapping force with laser power for a 1.5 W diode pumped Nd:YAG laser source for a single optical trap system. Non-linear trends below 80mW laser power are not used for extrapolation.

Usually, untrapped beads flow along the surface of the slide, making fluid velocity estimates difficult. Second, steady fluid flow is difficult to achieve for the lowest flow rates. Third, the scatter in calibration results is considerably greater than for the stage-movement technique. The stage-movement technique, used in the current study, provides a more accurate method to determine the velocity of the fluid from known stage velocity, thereby resolving the first two limitations of the fluid-chamber method.

The escape force over a range of laser powers is shown in Fig.2. The reported laser power is measured at the objective lens. At maximum power for the 1.5W laser, only 917 mW of laser power was measured due to losses through the optics. In our system, the stage velocity limits its direct calibration to a laser power of only about 300 mW. The escape force for values of higher laser power is linearly extrapolated from the calibration data in Fig. 2. At maximum laser power, corresponding to 917 mW, an escape force of 193 ± 20 pN is predicted. The linear relationship between laser power and escape force is consistent with theoretical predictions (Ashkin, 1992) and empirical findings (Svoboda and Block, 1994).

2.2 Sample Preparation

Blood samples from healthy adults are first obtained by a finger prick using a lancet device. The red blood cells are then isolated from the other blood components via a centrifugation process. Subsequently, silica microbeads are added to the isolated red blood cells in PBS with pH 7.4 and stored at 4 $^\circ$ C for 1 hour to allow for spontaneous and nonspecific binding of beads to cells. *In vitro* optical tweezers tests are then performed immediately. All preparations and tests are done at room temperature. The results presented in this paper are based on stretch test data from 16 different red blood cells.

2.3 Stretch Tests

Prepared red blood cells with attached silica microbeads are added to a solution of PBS and BSA. As the present experiment involves a single optical trap, one of the two microbeads is adhered to the glass slide while the other is trapped using the laser beam as shown in Fig. 3. This is accomplished by the addition of BSA, which limits microbead adhesion to the slide. Correct bead arrangement can be confirmed by trapping the microbead not attached to the slide. Because the optical trap is located above the slide surface and focal plane, a microbead that is successfully trapped will appear out of focus, indicating that the microbead is not adhered to the slide surface (see right bead in Fig 3 (b)). With this microbead trapped, the stage can be translated to determine if the other microbead is adhered to the slide. Adherence to the slide is confirmed if the adhered microbead moves in a manner consistent with the stage, unaffected by the forces induced by the trapped microbead. In fact, cell stretching is performed by this same method. With one microbead held fixed in the optical trap, moving the microscope stage, which in turn moves the microbead adhered to the glass slide, stretches the cell. A cell is stretched at different laser powers to record cell deformation over a range of forces. All stretch tests are recorded digitally for image analysis of cell deformation. For each stretch test, the axial diameter (in the direction of stretch) and transverse diameter (orthogonal to stretch direction) of the cell are measured from the still-frame image when the trapped bead just escapes the trap. The calibration of laser power to escape force (Fig. 2) determines the force at this instant. The cell diameters are measured from the still-frame image (Fig. 3). Notice that the axial diameter is actually the projected axial diameter because of the height difference

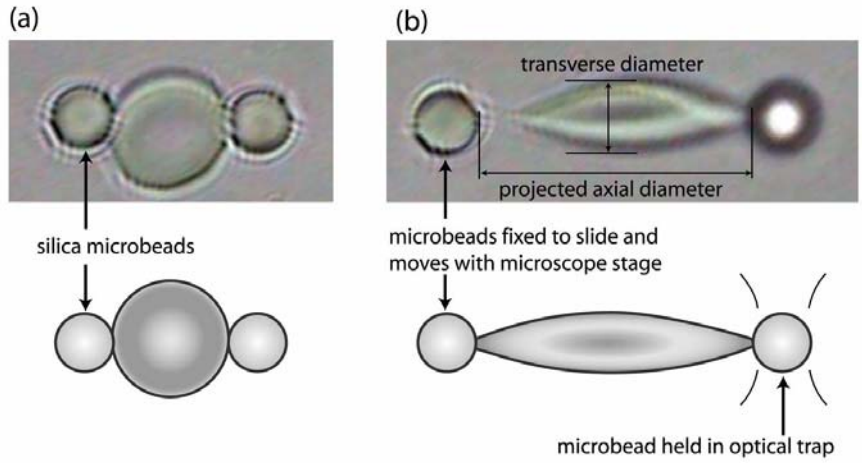

Figure 3 : Illustration of an optical trap method for cell stretching. Two silica microbeads, each 4.12 μm in diameter, are non-specifically attached to the red cell at diametrically opposite points. (a) The left bead is anchored to the surface of the glass slide. The optical image corresponds to the unstrained configuration. (b) The right bead is trapped using the optical tweezers. While the trapped bead remains stationary, moving the slide and attached left bead stretches the cell. The optical image shows an example of large deformation of a cell at 193 pN of force.

between the beads (Fig. 4). With the trapped bead height known, the actual axial cell diameter is calculated. Also, time dependent properties can be measured from the relaxation of the cell after the trapped bead escapes the trap. By measuring changes in axial and transverse diameters over time as the cell recovers its original shape, viscoelastic properties can be experimentally probed.

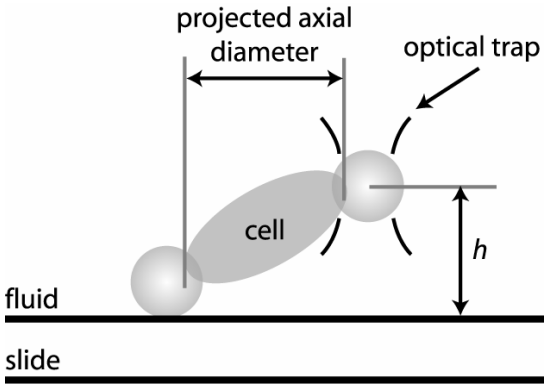

Figure 4 : Optical images of stretch tests show the projected axial diameter because of a height difference between trapped and attached beads. With the trapped bead height known, the actual axial cell diameter can be calculated.

3 Modeling of Deformation

The spectrin network which underlies the phospholipid bilayer of the human red blood cell is generally considered to impart shear resistance to the cell membrane although the bilayer itself has little resistance to shear deformation. As reviewed by Dao et al. (2003), the effective cell membrane which comprises the phospholipid bilayer and the spectrin network is usually modelled as an incompressible solid (Evans, 1973; Evans and Skalak, 1980) where the membrane shear stress T_s (expressed in units of force per unit length) is related to the principal stretch ratios, λ_1 and λ_2, as

$$T_s = 2\mu\gamma_s = \frac{\mu}{2}\left(\lambda_1^2 - \lambda_2^2\right), \tag{3a}$$

$$T_s = \frac{1}{2}\left(T_1 - T_2\right) \text{ and } \gamma_s \equiv \frac{1}{2}\left(\varepsilon_1 - \varepsilon_2\right) = \frac{1}{4}\left(\lambda_1^2 - \lambda_2^2\right) \tag{3b}$$

$$\lambda_1\lambda_2 = 1 \tag{3c}$$

where T_1 and T_2 are the in-plane principal membrane stresses, ε_1 and ε_2 are the in-plane principal Green's strains of the membrane, μ is the membrane shear modulus (assumed to be constant and expressed in units of force per unit length) and γ_s is the shear strain. The assumption of a constant area for the cell membrane is usually invoked, as indicated by equation (3c).

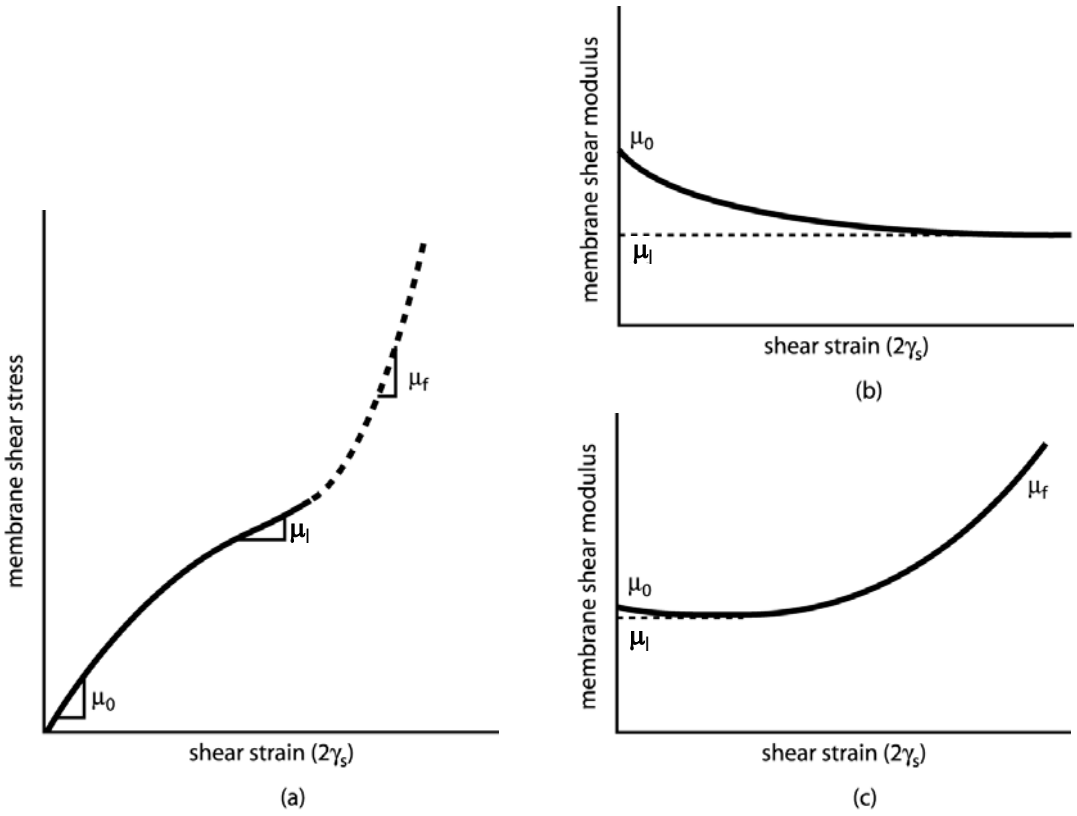

Figure 5 : Schematic illustration of the hyperelastic constitutive response used in some of the computational simulations. (a) Uniaxial stress-strain response. (b) The variation of the membrane shear modulus with the progression of deformation of the first order hyperelasticity model, where strains are representative of the large deformation response achieved in the present optical tweezer experiments. (c) The variation of the membrane shear modulus with respect to shear strain of a higher order hyperelastic model.

Other possible constitutive models can also be explored in the context of the deformation of red blood cells. One such approach entails use of a hyperelastic effective material model for capturing the large deformation response of the membrane. Dao et al. (2003) used the simplest first order formulation using a one-parameter Neo-Hookean form where the strain energy potential function (Simo and Pister, 1984) is of the form,

$$U = \frac{G_0}{2}\left(\lambda_1^2+\lambda_2^2+\lambda_3^2-3\right), \tag{4a}$$

where the assumption of incompressibility (constant volume) is also invoked. Here G_0 is the initial value of bulk shear modulus, and λ_i (i = 1-3) are the principal stretches. The incompressibility condition implies that $\lambda_1\lambda_2\lambda_3 = 1$. Further refinements to this approach are explored here by invoking a higher order formulation (a two-parameter Yeoh form (Yeoh, 1990)) whereby

$$U = \frac{G_0}{2}\left(\lambda_1^2+\lambda_2^2+\lambda_3^2-3\right)+C_3\left(\lambda_1^2+\lambda_2^2+\lambda_3^2-3\right)^3. \tag{4b}$$

In the computations, we take values of the parameter C_3 to be those which best match experimental data ($C_3 = G_0/30$ in the current study). The potential function Udefines the nonlinear elastic stress-strain behavior. When the initial membrane thickness is h_0, the constitutive description of eqs. (4) results in the initial in-plane membrane shear modulus $\mu_0 = G_0h_0$. Figure 5(a) schematically shows the uniaxial stress-strain response of such a neo-Hookean hyperelastic material, the membrane elasticity modulus typically decreases from its initially high value, μ_0, to a relatively smaller value, μ_l, at larger strains, before attaining a higher value, μ_f, again

prior to final failure. The slope of the membrane shear stress (T_s) versus shear strain ($2\gamma_s$) is therefore initially a decreasing function of shear strain (see Fig. 5(b)) and eventually a rapidly increasing function of shear strain (see Fig. 5(c)). For the simple first order neo-Hookean material described by eq. (4a), only the first stage (μ_0) and the second stage (μ_l) will be considered subsequently. For the higher order response described by eq. (4b), the first stage (μ_0) and the third stage (μ_f) will be the most important characteristic regions described. Specifically, μ_l (for the Neo-Hookean description) or μ_f (for the Yeoh description) is taken here at a relatively large stretch ratio of $\lambda_1 = 3$ or 2 respectively under direct uniaxial tension. The neo-Hookean rubber elasticity model for the membrane entails two material parameters: the initial shear modulus μ_0 and the second stage, large deformation modulus μ_l. In the current first order model, choice of one value of the two parameters also determines the other; while introducing higher order term C_3 results in independent variations of μ_0 and μ_f, see Figure 5(c). Choice of values for these parameters, which facilitate the matching of computational predictions with experimental results, has been systematically explored, and reported in this paper and in Dao et al (2003).

When the constant membrane area constraint, i.e. $\lambda_1\lambda_2 = 1$ (where $\lambda_3 = 1$), is added to eq. (4a), the constitutive description of eq. (4a) is equivalent to that of eq. (3). With this additional constraint, the in-plane membrane shear modulus stays at a constant value of $\mu = G_0 h_0$ throughout the entire deformation history (Dao et al, 2003).

While the foregoing analytical descriptions for the thin shell employ a single material property, i.e., the membrane shear modulus, more comprehensive analyses involving computational simulations of cell deformation invoke another material parameter in addition to the in-plane shear modulus μ: the bending modulus B. It is generally known that the contribution to the uniaxial tensile elastic deformation of the red blood cell from the bending modulus is much less than that from the shear modulus. Therefore, a typical (fixed) value of $B = 2\text{x}10^{-19}$ N·m is assumed in all the computations unless specified otherwise. We match the computational simulations with experimentally observed evolution of axial and transverse cell diameter at different forces imposed by the optical tweezers, and then extract shear modulus on the basis of the foregoing constitutive assumptions.

Computational simulations of large deformation stretching of the cell by optical tweezers were performed using three-dimensional finite element analysis of the biconcave red blood cell containing the cytosol in the interior. Because of symmetry in the optical tweezers loading geometry, it suffices to simulate one half of the cell contacted by a bead. Symmetric boundary conditions with 12,000 three-dimensional shell elements were employed in the simulations using the general purpose finite element program, ABAQUS (ABAQUS, 2002). Full details of the computations can be found in Dao et al. (2003). As noted there, the volume of the fluid inside the cell was kept constant in the simulations.

4 Results

Figure 6 shows that observed shape changes are matched by computation when μ_0 was assumed to be 7.3 μN/m (with $\mu_f = 19.2$ μN/m) using a higher order hyperelastic model described by eq. (4b). The contact size, d_c, was taken to be 2 μm in this set of calculations. The left column in the figure is a sequence of optical images revealing large deformation response of the red blood cell at different stretching forces. At 193 pN, the axial diameter of the cell increases by 50% and the transverse diameter is reduced by more than 40%. The middle column shows contours of constant maximum principal strain at corresponding stretching forces; logarithmic strains at sites of contact between the cell and the beads can reach values of approximately 100% at a stretching force of 193 pN. The right column shows one half of the computed full three-dimensional shape of the cell at different imposed forces; the structural folding observed at large strains appears to contribute significantly towards the shrinking in the transverse direction. Evidence of such folding is also seen experimentally, as for example in the lower images in the left column of Fig. 6.

Note that in the original results reported by Dao et al (2003) and Lim et al (2004), the maximum forces imposed on the cell were estimated to be on the order of 400 pN. These original estimates were subsequently revised and corrected in corrigenda to the original publications, on the basis of recalibration and new experimental data which revealed lower maximum forces. Here we include only the revised and corrected experimental data.

Comparisons of predicted and measured changes in axial and transverse diameters of the cell using the neo-Hookean model in eq. (4a) are plotted in Fig. 7 for $\mu_0 =$ 5.3, 7.3 and 11.3 μN/m (with $\mu_l = 2.4$, 3.3 and 5.0 μN/m,

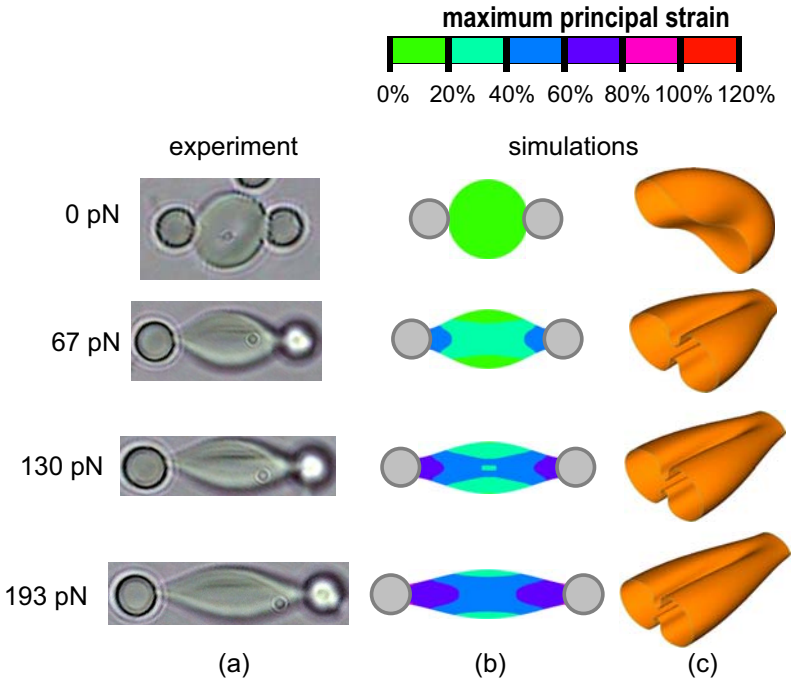

Figure 6 : Images of the red cell being stretched from 0 pN to 193 pN. The images in the left column are obtained from experimental video photography whereas the images in the center column (top view) and in the right column (half model 3D view) correspond to large deformation computational simulation of the biconcave red cell (with μ_0 = 7.3 μN/m, μ_f = 19.2 μN/m). The middle column shows a plan view of the stretched biconcave cell undergoing large deformation at the forces indicated on the left. The predicted shape changes are in reasonable agreement with observations. The color contours in the middle column represent spatial variation of constant maximum principal strain. The right column shows one half of the full three-dimensional shape of the cell at different imposed forces; here, the membrane was assumed to contain a fluid, which preserved the internal volume.

respectively). Again the contact size d_c was taken to be 2 μm. Simulations capture experimental trends over the range of 0–88 pN load well, while they deviate towards the softer side gradually after 88 pN load. Alternatively, if we invoke the constitutive response given in eq. (3) with constant area for the cell membrane in our three-dimensional computational simulation, a fixed value of the membrane shear modulus, $\mu_0 = \mu_l = \mu_f = 5.5$ μN/m appears to match the average values of our experimental observations of variations in axial and transverse diameter of the cell with the applied force within the 0-88 pN range (see Fig. 7). In the computational images, the existence of the cytosol inside the membrane prevents contact between the upper and lower surfaces. From the experimental evidence and computational results, significant membrane folding was often observed similar to those shown in Fig. 6 (left column and right column).

Comparisons of predicted and measured changes in axial and transverse diameters of the cell using the higher order Yeoh model in eq. (4b) are plotted in Fig. 8 for μ_0 = 5.3, 7.3 and 11.3 μN/m (with μ_f = 13.9, 19.2 and 29.6 μN/m, respectively). Again the contact size d_c was taken to be 2 μm. Simulations capture experimental trends over the entire range of experimental data well, including the small deformation range and the error bars. Comparing Figs. 7 and 8, it is seen that the higher order model apparently provides a much better match with experiments at high stretching ratios than the first order hyperelastic model.

The in-plane shear modulus μ_0 = 5.3–11.3 μN/m, and μ_l = 2.4–5.0 μN/m estimated from the experimental results and simulations reported in this paper are lower than the earlier values predicated upon higher optical force assumptions. The present corrected values are comparable to the range of 4.0–10 μN/m reported in the literature where the estimates have been principally based on

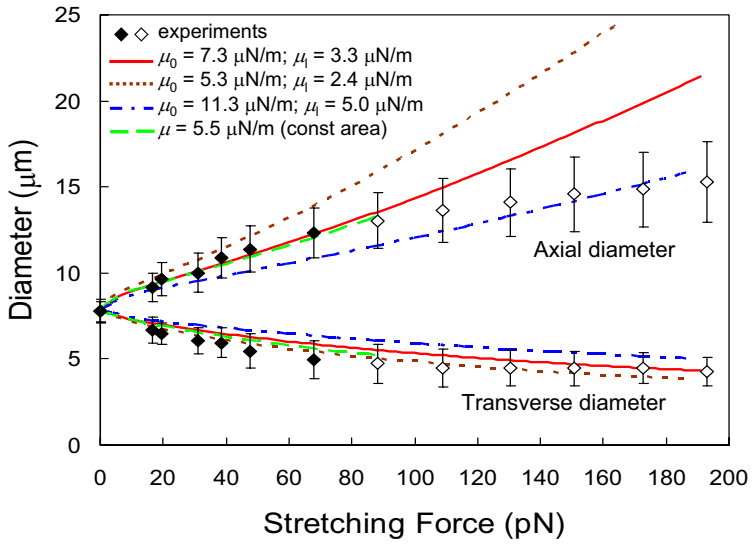

Figure 7 : Variation of measured axial and transverse diameter (solid line with scatter band) of red cell against stretching force of optical tweezers during large deformation. The dotted, solid and dash-dotted lines represent computational predictions for the axial/transverse diameter with μ_0= 5.3, 7.3 and 11.3 μN/m, and with μ_l= 2.4, 3.3 and 5.0 μN/m, respectively, invoking the neo-Hookean first order hyperelastic constitutive response, eq. (4a), which assumes constant volume. The computational model uses the three-dimensional biconcave disk with a contact diameter of 2 μm. Also shown are the predictions of simulations assuming constant membrane area, represented by long dashed lines, using the model given by eq. (3).

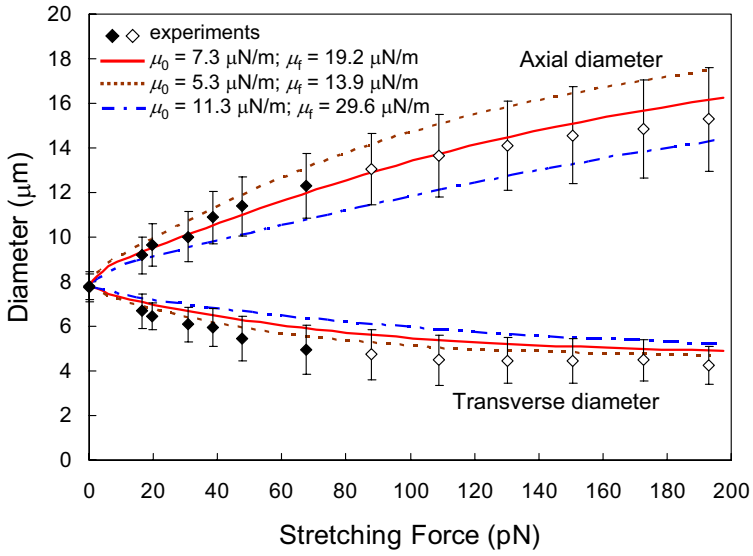

Figure 8 : Variation of measured axial and transverse diameter (solid line with scatter band) of red cell against stretching force of optical tweezers during large deformation. The dotted, solid and dash-dotted lines represent computational predictions for the axial/transverse diameter with μ_0= 5.3, 7.3 and 11.3 μN/m, and with μ_f= 13.9, 19.2 and 29.6 μN/m, respectively, invoking a higher order hyperelastic constitutive response, eq. (4b), which assumes constant volume. The computational model uses the three-dimensional biconcave disk with a contact diameter of 2 μm.

micropipette aspiration experiments. These values are also more in line with expectations than those derived from the earlier optical tweezers studies of Hénon et al (1999) and Sleep et al (1999) for small elastic deformation, indicating that possible effects of calibration as well as analysis of the data may have influenced the inference of elastic properties extracted from these optical tweezers experiments.

Video images of the elastic relaxation response of the stretched cell upon release of the force induced by stretching with optical tweezers can be used to infer the viscoelastic properties of the cell membrane. Hochmuth et al (1979) estimated the recovery characteristic time t_c of the red blood cell to be

$$\frac{\left(\lambda_1^2-1\right)\left(\lambda_{1,\max}^2+1\right)}{\left(\lambda_1^2+1\right)\left(\lambda_{1,\max}^2-1\right)}=\exp\left(-\frac{t}{t_c}\right) \tag{5}$$

where $\lambda_{1,\max}$ is the initial (maximum) value of the stretch ratio of the red cell and the characteristic time for relaxation is given by

$$t_c=\frac{\eta}{\mu} \tag{6}$$

where η is the coefficient of surface viscosity of the cell membrane, and μ is the in-plane shear modulus of the membrane. Figure 9 shows the corresponding best fit to the experimental data on relaxation using eq. (5). Using relaxation data from eight different experiments, the characteristic time is estimated to be $t_c=0.19\pm0.06$ s. It is of interest to note here that micropipette aspiration experiments have led to estimates of characteristic time of relaxation from large deformation of the red blood cell to be in the range 0.10–0.30 s (Chien et al 1978; Hochmuth 1987). With membrane shear modulus μ taken to be approximately 2.4-11.3 μN/m, the corresponding membrane viscosity, η, calculated from eq. (6) and Fig. 9 is about 0.3 to 2.8 (μN/m)·s, which compares well with the literature values of 0.6 to 2.7 (μN/m)·s found using micropipette experiments (Hochmuth 1987).

Three-dimensional computational simulations of the loading response are performed by incorporating the viscoelastic term to the constitutive behavior of the cell membrane by modifying eq. (3) as (Evans and Hochmuth, 1987; Dao et al, 2003),

$$T_s=\frac{\mu}{2}\left(\lambda_1^2-\lambda_1^{-2}\right)+2\eta\frac{\partial \ln\lambda_1}{\partial t} \tag{7}$$

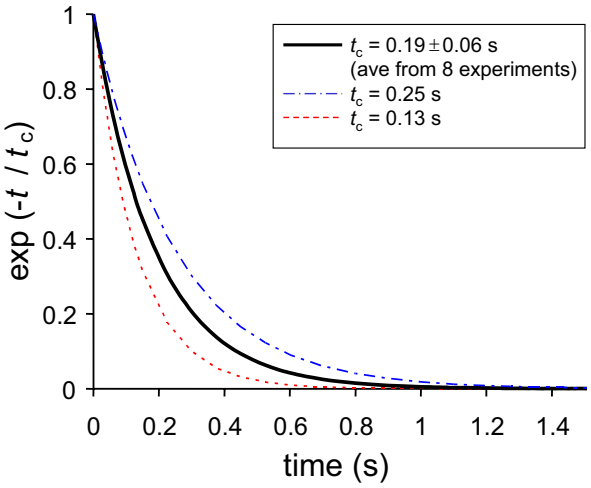

Figure 9 : Best fit to the experimental relaxation data. Using relaxation data from eight different experiments, the characteristic time was estimated to be $t_c=0.19\pm0.06$s using eq. (6).

where t is time, and t_c is the characteristic time for relaxation. For $t_c=0.19$ s and an estimated stretch rate of $\dot{\lambda}_1=0.3$ s^{-1}, the error caused by ignoring membrane viscosity during the loading stage is found to be negligibly small.

5 Concluding Remarks

In this paper, we have presented a critical assessment of recent advances in the use of the optical tweezers method for the study of single living cells. Through new experimental data, calibration methods and three-dimensional computational modelling, it is also shown that direct *in vitro* force-displacement relationships for human red bloods can be obtained reproducibly from such experiments by deforming the cells at large elastic strains. It is further demonstrated that the elastic properties of the human red blood cell, particularly the in-plane shear modulus, estimated from the large deformation optical tweezers experiments falls within the range of values derived from prior studies that made use of the micropipette aspiration experiments. These findings of the present work modify earlier claims that employed optical tweezers for cell deformation where apparent artefacts from calibration methods and/or interpretation of experiments could have contributed to the inferred differences in elastic properties. The characteristic time for viscoelastic relax-

ation inferred from the optical tweezers method is also consistent with those estimated from micropipette aspiration experiments.

The results so established in this paper provide additional opportunities for the application of the optical tweezers technique for further study of single cell mechanics. For example, the feasibility to obtain direct force–extension curves using this method provides new possibilities for the systematic and quantitative investigation of the effects of disease states on mechanical response of living cells. With this information, the connections among elastic or viscoelastic properties of the cell, the chemical/biochemical environment of the cell and the onset and progression of diseases can be studied with a level of precision which may not be attainable with other experimental methods. Recent experimental studies by Mills et al (2004) on the infestation of human red blood cells by *Plasmodium falciparum* malaria parasites have demonstrated that reproducible force–extension curves providing critical quantitative insights into the effects of parasite maturation inside the cell on the elastic and viscoelastic responses could be extracted from the optical tweezers method. This technique could circumvent some of the experimental difficulties in probing the deformation characteristics of malaria-infected cells through micropipette aspiration where cell rigidity and enhanced adhesion of the cell membrane to the glass surface could lead to significant uncertainty and scatter in experimental data (e.g., Glenister et al, 2002). As noted earlier, the optical tweezers method also affords the flexibility to explore deformation characteristics under different well-controlled stress states which can be induced through the use of multiple beads that are strategically attached to the cell membrane for trapping and stretching.

The three-dimensional modelling approach outlined in this paper is predicated upon a continuum formulation. It is of interest to note that quantitative analysis of mechanical deformation by optical tweezers have also been performed by recourse to molecular level modelling of the spectrin network (Li et al, 2004). These simulations provide estimates of elastic properties which are consistent with experimental observations.

Acknowledgement: This work was supported by the Nano Biomechanics Lab, Division of Bioengineering at the National University of Singapore and the Laboratory for Experimental and Computational Micromechanics at the Massachusetts Institute of Technology (MIT). Partial funding of this work was provided by the Singapore-MIT Alliance, and a Faculty of Engineering Research Grant from NUS.

Supplementary Material

Video images of computational simulations of deformation of the human red blood cell during optical tweezers stretching are posted on the website which can be accessed through the electronic archive of this paper.

References

ABAQUS_Inc. (2002): ABAQUS User's Manual, Version 6.3, ABAQUS, Inc., Pawtucket, RI, USA.

Ashkin, A.; Dziedzic, J. M.; Yamane, T. (1987): Optical Trapping and Manipulation of Single Cells Using Infrared-Laser Beams. *Nature* 330, 769-771.

Ashkin, A.; Schutze, K.; Dziedzic, J. M.; Euteneuer, U.; Schliwa, M. (1990): Force generation of organelle transport measured in vivo by an infrared laser trap. *Nature* 348, 346-348.

Bao, G.; Suresh, S. (2003): Cell and molecular mechanics of biological materials. *Nature Materials* 2, 715-725.

Boal, D. (2002): Mechanics of the Cell, Cambridge University Press, Cambridge, U.K.

Bronkhorst, P. J. H.; Streekstra, G. J.; Grimbergen, J.; Nijhof, E. J.; Sixma, J. J.; Brakenhoff, G. J. (1995): A new method to study shape recovery of red blood cells using multiple optical trapping. *Biophys. J.* 69, 1666-1673.

Chien, S.; Sung, K. L. P.; Skalak, R.; Usami, S. (1978): Theoretical and Experimental Studies on Viscoelastic Properties Erythrocyte-Membrane. *Biophys. J.* 24, 463-487.

Dao, M.; Lim, C. T.; Suresh, S. (2003): Mechanics of the human red blood cell deformed by optical tweezers. *J. Mech. Phys. Solids* 51, 2259-2280.

Discher, D. E.; Boal, D. H.; Boey, S. K. (1998): Simulations of the erythrocyte cytoskeleton at large deformation. II. Micropipette aspiration. *Biophys. J.* 75, 1584-1597.

Evans, E. A. (1973): New Membrane Concept Applied to Analysis of Fluid Shear- Deformed and Micropipet-Deformed Red Blood-Cells. *Biophys. J.* 13, 941-954.

Evans, E. A.; Skalak, R. (1980): Mechanics and Thermal Dynamics of Biomembranes, CRC Press, Inc., Boca Raton, Florida, USA.

Fung, Y. C. (1993): Biomechanics : mechanical properties of living tissues, Springer-Verlag, New York, USA.

Glenister, F. K.; Coppel, R. L.; Cowman, A. F.; Mohandas, N.; Cooke, B. M. (2002): Contribution of parasite proteins to altered mechanical properties of malaria-infected red blood cells. *Blood* 99, 1060-3.

Henon, S.; Lenormand, G.; Richert, A.; Gallet, F. (1999): A new determination of the shear modulus of the human erythrocyte membrane using optical tweezers. *Biophys. J.* 76, 1145-1151.

Hochmuth, R. M. (1987): Properties of Red Blood Cells. In *Handbook of Bioengineering*, (eds. R. Skalak and S. Chien), McGraw-Hill, Inc., New York, USA.

Hochmuth, R. M.; Worthy, P. R.; Evans, E. A. (1979): Red-Cell Extensional Recovery and the Determination of Membrane Viscosity. *Biophys. J.* 26, 101-114.

Kellermayer, M. S. Z.; Smith, S. B.; Bustamante, C.; Granzier, H. L. (1998): Complete Unfolding of the Titin Molecule under External Force. *Journal of Structural Biology* 122, 197-205.

Li, J.; Dao, M.; Lim, C. T.; Suresh, S. (2004): Spectrin-Level Analysis of Shape Evolution and Large Deformation Elasticity of the Erythrocyte. *Manuscript in preparation*.

Lim, C. T.; Dao, M.; Suresh, S.; Sow, C. H.; Chew, K. T. (2004): Large deformation of living cells using laser traps. *Acta Materialia* 52, 1837-1845. See also corrigendum (2004): Acta Materialia 52, 4065-4066.

Mills, J. P.; Qie, L.; Dao, M.; Tan, K.; Lim, C. T.; Suresh, S. (2004): Direct force-displacement responses of red blood cells altered by different stages of *Plasmodium falciparum* malaria infection. *Manuscript in preparation*.

Parker, K. H.; Winlove, C. P. (1999): The deformation of spherical vesicles with permeable, constant- area membranes: Application to the red blood cell. *Biophys. J.* 77, 3096-3107.

Simmons, R. M.; Finer, J. T.; Chu, S.; Spudich, J. A. (1996): Quantitative measurements of force and displacement using an optical trap. *Biophysical Journal* 70, 1813-1822.

Simo, J. C.; Pister, K. S. (1984): Remarks on Rate Constitutive-Equations for Finite Deformation Problems - Computational Implications. *Computer Methods in Applied Mechanics and Engineering* 46, 201-215.

Sleep, J.; Wilson, D.; Simmons, R.; Gratzer, W. (1999): Elasticity of the red cell membrane and its relation to hemolytic disorders: An optical tweezers study. *Biophys. J.* 77, 3085-3095.

Svoboda, K.; Block, S. M. (1994): Biological Applications of Optical Forces. *Annual Review of Biophysics and Biomolecular Structure* 23, 247-285.

Svoboda, K.; Schmidt, C. F.; Branton, D.; Block, S. M. (1992): Elastic Properties of Extracted Red-Blood-Cell Membrane Skeletons. *Faseb Journal* 6, A523-A523.

Van Vliet, K. J.; Bao, G.; Suresh, S. (2003): The biomechanics toolbox: experimental approaches for living cells and biomolecules. *Acta Materialia* 51, 5881-5905.

Yeoh, O. H. (1990): Characterization of Elastic Properties of Carbon-Black-Filled Rubber Vulcanizates. *Rubber Chem. Technol.* 63, 792-805.